Applied Mathematics Letters 145 (2023) 108781

Contents lists available at ScienceDirect

Applied Mathematics Letters

www.elsevier.com/locate/aml

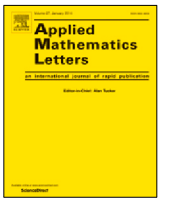

Parsimonious models of in-host viral dynamics and immune response

Hannah Lu [a], Francesco Giannino [b], Daniel M. Tartakovsky [c,*]

[a] *Department of Aeronautics and Astronautics, Massachusetts Institute of Technology, Cambridge, MA 02139, USA*
[b] *Department of Agricultural Sciences, University of Naples Federico II, Portici (NA), 80055, Italy*
[c] *Department of Energy Science and Engineering, Stanford University, Stanford, CA 94305, USA*

ARTICLE INFO

Article history:
Received 30 March 2023
Received in revised form 30 June 2023
Accepted 1 July 2023
Available online 7 July 2023

Keywords:
Identifiability
Virus dynamics
Immune response
COVID-19

ABSTRACT

Mathematical models of in-host viral dynamics and immune response are a vital tool for patient-specific estimation of the initial viral load, prediction of the course of an infection, etc. The COVID-19 pandemics has given impetus to the development of models with an ever-increasing degree of complexity. We show that one of the most popular models—the Target Cell Limited model—fails the identifiability test, i.e., its parameters cannot be uniquely inferred from readily available data such as viral load measurements. We present a model that is both identifiable and parsimonious according to information criteria. Our model's predictions match both reported observations of COVID-19 patients and predictions of its more complex counterparts.

1. Introduction

Like any mathematical conceptualization, models of the in-host SARS-CoV-2 virus dynamics and immune response involve system parameters. More often than not, these are not directly measurable and have to be inferred from observations of the system states; the ability to do so distinguishes identifiable models from unidentifiable ones [1]. While there are many such models developed at the epidemiological level [2–6], in-host models of the SARS-CoV-2 virus dynamics and immune response to infection in humans are relatively scarce [7–9]. This is partly due to several challenges in collecting and analyzing the observational data. To begin with, very few patients have long enough serial data points for a complete period including virus invasion and immune response. Observational studies [10,11] show that the peak viral load occurs in the early phase of illness, which is difficulty to capture because it is close to the time of symptom onset. The time to viral clearance also varies from weeks to months [12,13]. Moreover, the viral load dynamics exhibit various patterns depending on the disease severity [14,15] and patient's characteristics [16–18] such as gender, age, obesity, chronic diseases, mortality, etc.

* Corresponding author.
E-mail address: tartakovsky@stanford.edu (D.M. Tartakovsky).

https://doi.org/10.1016/j.aml.2023.108781
0893-9659/

2. Mathematical models

We start by describing in Section 2.1 a model of in-host viral dynamics and immune response, which was recently promulgated in connection with the COVID-19 epidemics [7–9]. Our model, proposed in Section 2.2, is inspired by Marchuk's model [19].

2.1. Target cell limited (TCL) model with immune response

In addition to target cells (T), infected cells (I) and free virus (V), this model accounts for interferon or IFN (with concentration F) and uninfected cells (with concentration R) that are refractory to infections because of IFN-induced antiviral effect. This gives rise to a system of five ordinary differential equations (ODEs),

$$\begin{cases} \dfrac{\mathrm{d}T}{\mathrm{d}t} = -\beta VT - \phi FT + \rho R \\ \dfrac{\mathrm{d}I}{\mathrm{d}t} = \beta VT - \delta I - \kappa IF \\ \dfrac{\mathrm{d}R}{\mathrm{d}t} = \phi FT - \rho R \\ \dfrac{\mathrm{d}V}{\mathrm{d}t} = pI - cV \\ \dfrac{\mathrm{d}F}{\mathrm{d}t} = qI - dF. \end{cases} \tag{1}$$

The rate at which the uninfected cells become refractory to infection is ϕFT, while the cells in the refractory state revert to the susceptible state at rate ρ. Prior to the emergence of the virus-specific adaptive immune response, the death rate of the infected cells is constant, δ_0. After the adaptive immune response emerges, the death rate increases with time as described by the time-dependent coefficient $\delta(t) = \delta_0 e^{\sigma(t-\mu)}$; here, μ is the time at which the adaptive immune response emerges, and σ determines how fast it saturates. To be specific, δ_0 is assumed to be 1. The mass action term κIF represents the clearance of infected cells by natural killer cells, which are activated by IFN and are proportional to the level of IFN. Finally, IFN is secreted by infected cells at rate q and decays at rate d.

2.2. Proposed model

Driven by the principle of parsimony, we formulate a relatively simple mathematical model that is as accurate in representing the in-host dynamics of SARS-CoV-2 infection as its recent counterparts. Our model, a modification of the venerable Marchuk model for infectious disease [19], consists of three ODEs,

$$\begin{cases} \dfrac{\mathrm{d}V}{\mathrm{d}t} = \beta V - \gamma AV, \\ \dfrac{\mathrm{d}C}{\mathrm{d}t} = \alpha AV - \mu_C(C - C^*), \\ \dfrac{\mathrm{d}A}{\mathrm{d}t} = \rho C - \eta\gamma AV - \mu_A A. \end{cases} \tag{2}$$

It describes the temporal evolution of viral load $V(t)$, plasma cell concentration $C(t)$, and antibody concentration $A(t)$. The dynamics is controlled by the virus multiplication coefficient β; the probability for a virus to be neutralized after encountering the antibodies, expressed by the coefficient γ; the plasma cell life time, $1/\mu_C$; the decay time of antibodies, $1/\mu_A$; the normal level of plasma cells in a healthy organism, C^*; the rate of antibodies production by one plasma cell, ρ; the number antibodies required to neutralize one virus, η; and the probability of virus-antibody collision reflected in the coefficient $\alpha(t) = \alpha_0 \exp(\sigma_0 t^2 + \sigma_1 t)$.

Our model employs the simplest hypothesis on the formation of cascade populations of plasma cells [19, Sec. 2.1], such that the plasma cell growth is proportional to AV. The time-dependence of α mimics the delayed function due to plasma cell formation lag in the original Marchuk model. The last ODE in (2) represents a balance of the number of antibodies reacting with virus, such that the terms $\eta\gamma AV$ and $\mu_A A$ represent the consumption of antibodies in virus elimination and the drop in the antibodies population due to their aging, respectively.

3. Experimental data

We analyze data from eight patients who were part of a larger cohort of epidemiologically linked cases (i.e., infected from a known close contact to an index case), which occurred after January 23, 2020 in Munich [20]. All the patients were treated in a single hospital after initial diagnostic testing and all virological tests were repeated daily after admission by the same standards for PCR with reverse transcription (RT-PCR). The clinical characteristics of the patients—all of whom were young-to-middle-aged professionals without notable underlying diseases—showed comparatively mild symptoms. The viral load measured in RNA copies per ml from the specimens of sputum in the dataset [20] provides more informative virus kinetics than the specimens of throat swab and stool during the observation period—with higher detection rates, a delayed peak, and slower decline.

These clinical observations show that the sputum viral loads present a late second peak around 10 days after the first peak in several patients who exhibited some signs of lung infection, indicating one important feature of the viral dynamics [20]. Therefore, the viral RNA concentrations in sputum are used for parameter fitting in all the mathematical models considered.

4. Model comparison

A major challenge in virus dynamics modeling, and the one that eludes the TCL model, is to capture the bimodal viral load peaks, which appear in most COVID-19 patients in the dataset [20] and in other infectious diseases [21–24]. The model in (1), which adds the effect of IFN and the refractory cells to the TCL model, can generate a viral plateau/second peak. Consequently, it satisfactorily fits the experimental data from ponies infected with H3N8 in [21]. Thus, we compare our model (2) with the reference model (1) on the same dataset [20] from the following two perspectives.

4.1. Parameter identification

We estimate the model parameters in (2) and the initial viral load $V(0)$ by fitting the model prediction to the viral load data from [20]. Our model deals with the combined population of immunocompetent and antibody-producing cells, whose concentration is $C(t)$. If an organism had no information about a given antigen and therefore had no immunocompetent cells to fight it, then $C(0) = 0$. In that case, a more evolved mathematical model would be needed to initiate the cascade of reactions, which involve immunocompetent cells with specific receptors capable of provoking an immune response to the antigen. For simplicity, we omit the starting mechanism and assume that an organism has a nonzero normal level of plasma cells $C(0) = C^* > 0$ and nonzero antibody $A(0) = 0.1$ at the beginning of the infection. Moreover, for fitting purposes, we replace $C(t)$ in (2) with its scaled counterpart $\tilde{C}(t) = C(t)/C^*$ for which $\tilde{C}^* = 1$. Following [19] and others, we set $\rho = 4\mu_A$, i.e., assume the ratio of production rate and natural death rate of the antibodies to be fixed. Similar assumptions are often used to analyze the characteristics of the immune response (e.g., [25]); experimental measurements can be designed to estimate this ratio (e.g., [26–28]).

The eight model parameters (plus one initial condition) in our model (2), and the ten parameters (plus one initial condition) in the competing model (1), are obtained via a maximum likelihood estimator, i.e., by minimizing the root mean square error, RMS $= [N^{-1}\sum_{i=1}^{N}(\ln v_i - \ln V_i)^2]^{1/2}$, between the measurements (v_i) and model predictions (V_i) of the viral load in an individual patient, The subscript i refers to the ith day after the patient's admission, with N denoting the total number of observations/days. This nonlinear minimization problem admits multiple minima; it is solved with the Matlab nonlinear least-squares solver `lsqnonlin`.

The issue of identifiability is an important factor in model selection. A mathematical model is identifiable if its parameters can be uniquely determined from the measurable output data; otherwise, the system is unidentifiable [1]. Identifiability guarantees a unique and precise interpretation of the parameters and unmeasured variables. Therefore, an identifiable model is superior to its unidentifiable counterpart, even if the former contains more parameters than the latter. We conduct the identifiability analysis for our model (2) and the competing model (1) in the following Theorem 1 and Theorem 2, respectively.

Theorem 1. *With the assumptions $\rho = 4\mu_A$ and the regularity of $V(t)$, all the model parameters in (2) are identifiable from measurements of the viral load $V(t)$ only, provided the minimum of 9 observations are available.*

Proof. The following proof employs the implicit function method [1] to investigate the identifiability of (2). Using the prime to indicate the derivative, we recast the third ODE in (2) as

$$C = \frac{1}{\rho}(A' + \mu_A A + \eta\gamma AV) \quad \text{and} \quad C' = \frac{1}{\rho}(A'' + \mu_A A' + \eta\gamma(AV)'). \tag{3}$$

Substitution of (3) into the second ODE in (2) yields

$$A'' = -\mu_A A' - \eta\gamma(AV)' + \alpha\rho AV - \mu_C A' - \mu_C\mu_A A - \mu_C\eta\gamma AV + \mu_C\rho. \tag{4}$$

The first ODE in (2) gives rise to

$$A = \frac{\beta}{\gamma} - \frac{1}{\gamma}\frac{V'}{V}, \quad A' = -\frac{1}{\gamma}\left(\frac{V'}{V}\right)', \quad A'' = -\frac{1}{\gamma}\left(\frac{V'}{V}\right)''. \tag{5}$$

Substituting (5) into (4), we obtain

$$\begin{aligned}\left(\frac{V'}{V}\right)'' + (\mu_A + \mu_C)\left(\frac{V'}{V}\right)' + \mu_C\mu_A\left(\frac{V'}{V}\right)' + \eta\gamma V'' \\ + (\mu_C\eta\gamma - \beta\eta\gamma - \alpha\rho)V' + (\alpha\rho\beta - \mu_C\eta\gamma\beta)V + (\mu_C\gamma\rho - \mu_C\mu_A\beta) = 0.\end{aligned} \tag{6}$$

Let us denote $\Theta = (\theta_1, \ldots, \theta_6)^\top$, where $\theta_1 = \mu_A + \mu_C$, $\theta_2 = \mu_A\mu_C$, $\theta_3 = \eta\gamma$, $\theta_4 = \mu_C\eta\gamma - \beta\eta\gamma - \alpha\rho$, $\theta_5 = \alpha\rho\beta - \mu_C\eta\gamma\beta$, and $\theta_6 = \mu_C\gamma\rho - \mu_C\mu_A\beta$. Then, the higher-order ($i \geq 3$) derivatives from (6) are

$$\left(\frac{V'}{V}\right)^{(i)} + \theta_1\left(\frac{V'}{V}\right)^{(i-1)} + \theta_2\left(\frac{V'}{V}\right)^{(i-2)} + \theta_3 V^{(i)} + \theta_4 V^{(i-1)} + \theta_5 V^{(i-2)} + \theta_6 = 0. \tag{7}$$

The parameters Θ are computed from any persistently exciting trajectory $V(t)$ such that

$$\text{rank} = \begin{bmatrix} (V'/V)^{(1)} & V'/V & V^{(2)} & V^{(1)} & V & 1 \\ (V'/V)^{(2)} & (V'/V)^{(1)} & V^{(3)} & V^{(2)} & V^{(1)} & 0 \\ \vdots & \vdots & \vdots & \vdots & \vdots & \vdots \\ (V'/V)^{(6)} & (V'/V)^{(5)} & V^{(7)} & V^{(6)} & V^{(5)} & 0 \end{bmatrix} = 6. \tag{8}$$

Therefore, μ_C and μ_A are computed from θ_1 and θ_2 directly and β is solved using θ_3, θ_4 and θ_5 afterwards. Then, the parameters $\gamma, \eta, \alpha, \rho$ are identified in terms of the measurements and one remaining parameter. With the assumption $\rho = 4\mu_A$, all parameters are identified. The minimum number of required measurements of V is 9 since up to the 8th derivative of V is involved. □

Theorem 2. *All model parameters in (1) are not identifiable from measurements of the viral load $V(t)$, regardless of how many observations are available.*

Proof. Denote the parameter set of the reference model (1) by Θ. According to the implicit function method [1], one cannot find a function Φ such that $\Phi(\Theta, V, V^{(1)}, \dots, V^{(k)}) = 0$ for any integer k. An example is presented in Fig. 1: for $\Theta \neq \tilde{\Theta}$, the solutions share the same trajectories of $V(t)$. □

Remark 1. Following the same implicit function method, we show that all parameters in the reference model (1) are identifiable if both viral load and IFN measurements are available. At least 4 measurements of V and 5 measurements of F are required. This verifies that parameter identification for the reference model can provide a meaningful interpretation if both V and F can be measured, as in [21].

4.2. Model selection criteria

We compare the performance of the two alternative models of immune response in terms of the modified Akaike information criterion (AIC) [29], $\text{AIC} = 2M + N\ln(\text{RMS})^2 + 2M(M+1)/(N-M-1)$. Here, M is the number of fitting parameters in a given model, and RMS is the residual calculated during the fitting process. The principle of parsimony implies that the model with a lower AIC value fits the data better from a statistical viewpoint. Comparison between the models in (1) and (2) is performed individually for all patients, resulting in the AIC values reported in Table 1. A simpler model, i.e., a model with fewer variables and parameters, has a lower AIC and is preferable to a more complex model, provided their RMS errors are comparable.

5. Results

Our model (2) outperforms the reference model (1) in its ability to reproduce the viral load data for all patients. First, it has much lower AIC values, although the reference model has slightly smaller RMS errors in most cases (reported in Table 1). Second and more important, our model is identifiable while the reference model is not. We prove in Theorem 1 that all parameters in our model are identifiable from 9 or more measurements of the viral load. On the contrary, the reference model is unidentifiable regardless of how many viral load measurements are available (see Theorem 2). It can only be identified from other data types, e.g., from at least 4 measurements of the viral load and 5 measurements of the IFN or from prior information about a portion of the parameter set. While one can estimate the parameters in the reference model by minimizing the RMS, the results are nonunique and highly sensitive to the initial guess. This lack of identifiability means that two different sets of parameters give the same model predictions (Fig. 1). This introduces significant uncertainty in some parameters and unmeasured variables, and undermines the predictive power of the reference model. As a result, the reference model, though fitting data accurately in the sense of RMS errors, cannot provide meaningful interpretations of the patient-specific immune response.

6. Conclusion and discussion

We propose a three-equation model, which captures the observed viral load dynamics, including a plateau and a second peak, the two features found in many COVID-19 patients. Its predictions of antibody curves

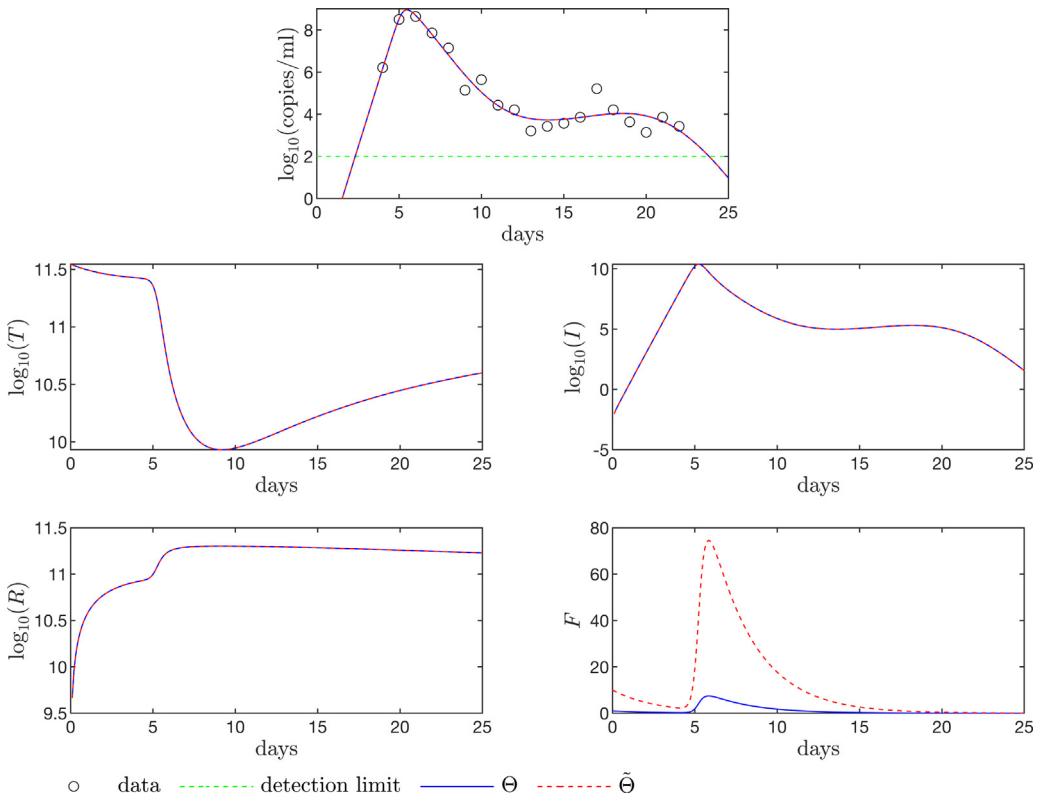

Fig. 1. Model predictions of virus load (V), target cells (T), infected cells (I), refractory cells (R) and IFN (F) from the best fit of the reference model, Eq. (1), for patient #1. The solid line is the simulation with the parameters in Table 2 and the dashed line is the simulation with the same parameters except for $\tilde{\phi} = 0.1\phi, \tilde{\kappa} = 0.1\kappa, \tilde{q} = 10q$ and $\tilde{F}_0 = 10F_0$.

Table 1
Quantitative measures of the predictive performance of our model (2) and the reference model (1).

Patient	Data points	RMS		AIC	
		Model (2)	Model (1)	Model (2)	Model (1)
1	19	0.5057	0.4579	12.0884	30.0336
2	18	0.7011	0.6335	27.7151	49.5688
3	18	0.5658	0.5341	19.9977	43.4200
4	9	0.8010	0.8231	−165.9948	−69.5044
7	20	0.9741	0.9622	34.9507	53.4579
8	14	0.8540	0.7951	58.5824	147.5803
10	16	1.2957	1.2946	61.7724	117.7463
14	8	0.5437	0.6493	−81.7488	−50.9109

are also consistent with observations. Our model is provably identifiable, while its commonly used alternative (dubbed as the reference model and given by (1)) is not. We also show that our model has a superior performance in terms of the AIC and, hence, is preferable to its competitors based on the principle of parsimony. The model can be used for more detailed studies of the within-host dynamics of viruses, cells, and antibodies. These may provide valuable information for future research on virus infection, treatment, and vaccination.

Since the dataset used to inform our model consists of relatively mild cases of COVID-19, we do not account for possible organ damage by assuming the immune system's efficiency to be independent of the severity of the disease. The organ damage can be incorporated into our model, as is done by Marchuk [19], providing a mathematical representation of "long Covid". Other limitations of our model can be ameliorated

by increasing its complexity. For example, our model represents the complexity caused by formation time of plasma cells via the time-dependent coefficient $\alpha(t)$, whose parameterization is valid for a certain infection period. Consequently, our model's predictions are less accurate before onset of symptoms and after virus clearance. The more complex Marchuk model describes these stages by employing ODEs with delay to represent the plasma cell formation lag. Identifiability (parameter identification) for delayed ODEs remains a challenge.

Data availability

Data will be made available on request.

Acknowledgments

This work was supported in part by Air Force Office of Scientific Research, United States under award number FA9550-21-1-038, by Office of Advanced Scientific Computing Research (ASCR) within the Department of Energy Office of Science under award number DE-SC0023163, and by National Science Foundation, United States under award 2100927.

Appendix A. Supplementary data

Supplementary material related to this article can be found online at https://doi.org/10.1016/j.aml.2023.108781.

References

[1] X. Xia, C.H. Moog, Identifiability of nonlinear systems with application to HIV/AIDS models, IEEE Trans. Automat. Control 48 (2) (2003) 330–336.
[2] A. Vespignani, H. Tian, C. Dye, J.O. Lloyd-Smith, R.M. Eggo, M. Shrestha, S.V. Scarpino, B. Gutierrez, M.U. Kraemer, J. Wu, et al., Modelling covid-19, Nature Rev. Phys. 2 (6) (2020) 279–281.
[3] A.J. Kucharski, T.W. Russell, C. Diamond, Y. Liu, J. Edmunds, S. Funk, R.M. Eggo, F. Sun, M. Jit, J.D. Munday, et al., Early dynamics of transmission and control of COVID-19: a mathematical modelling study, Lancet Infect. Dis. 20 (5) (2020) 553–558.
[4] G. Giordano, F. Blanchini, R. Bruno, P. Colaneri, A. Di Filippo, A. Di Matteo, M. Colaneri, Modelling the COVID-19 epidemic and implementation of population-wide interventions in Italy, Nature Med. 26 (6) (2020) 855–860.
[5] S. Moore, E.M. Hill, M.J. Tildesley, L. Dyson, M.J. Keeling, Vaccination and non-pharmaceutical interventions for COVID-19: a mathematical modelling study, Lancet Infect. Dis. 21 (6) (2021) 793–802.
[6] A.J. Kucharski, P. Klepac, A.J. Conlan, S.M. Kissler, M.L. Tang, H. Fry, J.R. Gog, W.J. Edmunds, J.C. Emery, G. Medley, et al., Effectiveness of isolation, testing, contact tracing, and physical distancing on reducing transmission of SARS-CoV-2 in different settings: a mathematical modelling study, Lancet Infect. Dis. 20 (10) (2020) 1151–1160.
[7] E.A. Hernandez-Vargas, J.X. Velasco-Hernandez, In-host mathematical modelling of COVID-19 in humans, Annu. Rev. Control 50 (2020) 448–456.
[8] S. Wang, Y. Pan, Q. Wang, H. Miao, A.N. Brown, L. Rong, Modeling the viral dynamics of SARS-CoV-2 infection, Math. Biosci. 328 (2020) 108438.
[9] N. Néant, G. Lingas, Q. Le Hingrat, J. Ghosn, I. Engelmann, Q. Lepiller, A. Gaymard, V. Ferré, C. Hartard, J.-C. Plantier, et al., Modeling SARS-CoV-2 viral kinetics and association with mortality in hospitalized patients from the French COVID cohort, Proc. Natl. Acad. Sci. 118 (8) (2021).
[10] S.A. Lauer, K.H. Grantz, Q. Bi, F.K. Jones, Q. Zheng, H.R. Meredith, A.S. Azman, N.G. Reich, J. Lessler, The incubation period of coronavirus disease 2019 (COVID-19) from publicly reported confirmed cases: estimation and application, Ann. Intern. Med. 172 (9) (2020) 577–582.
[11] X. He, E.H. Lau, P. Wu, X. Deng, J. Wang, X. Hao, Y.C. Lau, J.Y. Wong, Y. Guan, X. Tan, et al., Temporal dynamics in viral shedding and transmissibility of COVID-19, Nature Med. 26 (5) (2020) 672–675.
[12] M. Cevik, M. Tate, O. Lloyd, A.E. Maraolo, J. Schafers, A. Ho, SARS-CoV-2, SARS-CoV, and MERS-CoVand MERS-CoV viral load dynamics, duration of viral shedding, and infectiousness: a systematic review and meta-analysis, Lancet Microbe 2 (1) (2020) e13–e22.

[13] I.F.-N. Hung, V.C.-C. Cheng, X. Li, A.R. Tam, D.L.-L. Hung, K.H.-Y. Chiu, C.C.-Y. Yip, J.-P. Cai, D.T.-Y. Ho, S.-C. Wong, et al., SARS-CoV-2 shedding and seroconversion among passengers quarantined after disembarking a cruise ship: a case series, Lancet Infect. Dis. 20 (9) (2020) 1051–1060.
[14] Y. Liu, L.-M. Yan, L. Wan, T.-X. Xiang, A. Le, J.-M. Liu, M. Peiris, L.L. Poon, W. Zhang, Viral dynamics in mild and severe cases of COVID-19, Lancet Infect. Dis. 20 (6) (2020) 656–657.
[15] S. Zheng, J. Fan, F. Yu, B. Feng, B. Lou, Q. Zou, G. Xie, S. Lin, R. Wang, X. Yang, et al., Viral load dynamics and disease severity in patients infected with SARS-CoV-2 in Zhejiang province, China, January-March 2020: retrospective cohort study, Br. Med. J. 369 (2020) m1443.
[16] E.J. Williamson, A.J. Walker, K. Bhaskaran, S. Bacon, C. Bates, C.E. Morton, H.J. Curtis, A. Mehrkar, D. Evans, P. Inglesby, et al., Factors associated with COVID-19-related death using OpenSAFELY, Nature 584 (7821) (2020) 430–436.
[17] K. Wang, X. Zhang, J. Sun, J. Ye, F. Wang, J. Hua, H. Zhang, T. Shi, Q. Li, X. Wu, Differences of severe acute respiratory syndrome coronavirus 2 shedding duration in sputum and nasopharyngeal swab specimens among adult inpatients with coronavirus disease 2019, Chest 158 (5) (2020) 1876–1884.
[18] D. Yan, X.-Y. Liu, Y. n. Zhu, L. Huang, B. t. Dan, G. j. Zhang, Y. h. Gao, Factors associated with prolonged viral shedding and impact of lopinavir/ritonavir treatment in hospitalised non-critically ill patients with SARS-CoV-2 infection, Eur. Respir. J. 56 (1) (2020) 2000799.
[19] G.I. Marchuk, Mathematical Modelling of Immune Response in Infectious Diseases, Vol. 395, Springer Science & Business Media, 1997.
[20] R. Wölfel, V.M. Corman, W. Guggemos, M. Seilmaier, S. Zange, M.A. Müller, D. Niemeyer, T.C. Jones, P. Vollmar, C. Rothe, et al., Virological assessment of hospitalized patients with COVID-2019, Nature 581 (7809) (2020) 465–469.
[21] K.A. Pawelek, G.T. Huynh, M. Quinlivan, A. Cullinane, L. Rong, A.S. Perelson, Modeling within-host dynamics of influenza virus infection including immune responses, PLoS Comput. Biol. 8 (6) (2012) e1002588.
[22] B.R. Murphy, R.M. Chanock, M.L. Clements, W.C. Anthony, A.J. Sear, L.A. Cisneros, M.B. Rennels, E.H. Miller, R.E. Black, M.M. Levine, et al., Evaluation of A/Alaska/6/77 (H3N2) cold-adapted recombinant viruses derived from A/Ann Arbor/6/60 cold-adapted donor virus in adult seronegative volunteers, Infect. Immun. 32 (2) (1981) 693–697.
[23] B.R. Murphy, M.B. Rennels, R.G. Douglas Jr., R.F. Betts, R.B. Couch, T.R. Cate Jr., R.M. Chanock, A.P. Kendal, H.F. Maassab, S. Suwanagool, et al., Evaluation of influenza A/Hong Kong/123/77 (H1N1) ts-1A2 and cold-adapted recombinant viruses in seronegative adult volunteers, Infect. Immun. 29 (2) (1980) 348–355.
[24] R.L. Jao, E.F. Wheelock, G.G. Jackson, Production of interferon in volunteers infected with Asian influenza, J. Infec. Dis. 121 (4) (1970) 419–426.
[25] I. Pogozhev, R. Usmanov, S. Zuev, Models of processes in organism and population characteristics, 1993.
[26] M. Quinlivan, M. Nelly, M. Prendergast, C. Breathnach, D. Horohov, S. Arkins, Y.-W. Chiang, H.-J. Chu, T. Ng, A. Cullinane, Pro-inflammatory and antiviral cytokine expression in vaccinated and unvaccinated horses exposed to equine influenza virus, Vaccine 25 (41) (2007) 7056–7064.
[27] C. Lucas, J. Klein, M. Sundaram, F. Liu, P. Wong, J. Silva, T. Mao, J.E. Oh, M. Tokuyama, P. Lu, et al., Kinetics of antibody responses dictate covid-19 outcome, 2020, MedRxiv.
[28] R. Soleimani, M. Khourssaji, D. Gruson, H. Rodriguez-Villalobos, M. Berghmans, L. Belkhir, J.-C. Yombi, B. Kabamba-Mukadi, Clinical usefulness of fully automated chemiluminescent immunoassay for quantitative antibody measurements in covid-19 patients, J. Med. Virol. 93 (3) (2021) 1465–1477.
[29] K.P. Burnham, D.R. Anderson, Model Selection and Multimodel Inference: A Practical Information-Theoretic Approach, second ed., Springer-Verlag, NY, 2010.